JOURNAL OF INTEGRATED OMICS
A METHODOLOGICAL JOURNAL
HTTP://WWW.JIOMICS.COM

ORIGINAL ARTICLE | DOI: 10.5584/jiomics.v4i1.157

Subtoxic concentrations of benzo[*a*]pyrene induce metabolic changes and oxidative stress in non-activated and affect the mTOR pathway in activated Jurkat T cells

Sven Baumann[1,#], Maxie Rockstroh[2,#], Jörg Bartel[3], Jan Krumsiek[3], Wolfgang Otto[2], Harald Jungnickel[4], Sarah Potratz[4], Andreas Luch[4], Edith Wilscher[5], Fabian J. Theis[3,6], Martin von Bergen[1,2,7], Janina M. Tomm[2,*]

[1]Department of Metabolomics, Helmholtz-Centre for Environmental Research - UFZ, Permoser Str. 15, 04318 Leipzig, Germany; [2]Department of Proteomics, Helmholtz-Centre for Environmental Research - UFZ, Permoser Str. 15, 04318 Leipzig, Germany; [3]Institute of Bioinformatics and Systems Biology, Helmholtz Zentrum München, Ingolstädter Landstr. 1, 85764 Neuherberg, Germany; [4]Department of Product Safety, German Federal Institute for Risk assessment (BfR), Max-Dohrn Strasse 8-10, 10589 Berlin, Germany; [5]Interdisciplinary Centre for Bioinformatics, University of Leipzig, Härtelstr. 16-18, 04107 Leipzig, Germany; [6]Institute for Mathematical Sciences, TU München, Boltzmannstr. 3, 85747 Garching, Germany; [7]Aalborg University, Department of Biotechnology, Chemistry and Environmental Engineering, Aalborg University, Sohngaardsholmsvej 49, DK-9000 Aalborg, Denmark. [#] *contributed equally*

Received: 09 October 2013 **Accepted:** 26 December 2013 **Available Online**: 17 February 2014

Abstract

Recent studies have shown that aromatic compounds, such as B[*a*]P, influence the immune system even at low concentrations. Although the activation of immune cells is the first and thereby pivotal step in the immunological cascade, the current knowledge about the impact of environmental pollutants on this process is quite limited. Therefore, we investigated the effect of a subtoxic B[*a*]P concentration (50 nM) on the proteome and the metabolome of non-activated and activated Jurkat T cells. The GeLC-MS/MS analysis yielded 2624 unambiguously identified proteins. In addition to typical regulatory pathways associated with T cell activation, pathway analysis by Ingenuity IPA revealed several metabolic processes, for instance purine and pyruvate metabolism. The activation process seems to be influenced by B[*a*]P suggesting an important role of the mTOR pathway in the cellular adaptation. B[*a*]P exposure of non-activated Jurkat cells induced signaling pathways such as protein ubiquitination and NRF2 mediated oxidative stress response as well as metabolic adaptations involving pyruvate, purine and fatty acid metabolism. Thus, we validated the proteome results by determining the concentrations of 183 metabolites with FIA-MS/MS and IC-MS/MS. Furthermore, we were able to show that Jurkat cells metabolize B[*a*]P to B[*a*]P-1,6-dione. The combined evaluation of proteome and metabolome data with an integrated, genome-scale metabolic model provided novel systems biological insights into the complex relation between metabolic and proteomic processes in Jurkat T cells during activation and subtoxic chemical exposure.

Keywords: benzo[*a*]pyrene; antioxidant response element; *Jurkat T cell; activation; LC-MS/MS; Biocrates*.

Abbreviations

AhR: aryl hydrocarbon receptor; **APC**: antigen presenting cell; **APCI**: atmospheric-pressure chemical ionization; **ARE**: antioxidant response element; **B[*a*]P**: benzo[*a*]pyrene; **FDR**: false discovery rate; **FIA-MS/MS**: flow injection assay mass spectrometry; **GeLC-MS/MS**: 1D PAGE protein separation followed by liquid chromatography-tandem mass spectrometry; **IC-MS/MS**: ion chromatography coupled to mass spectrometry; **IL-2**: interleukin-2; **mTOR**: mammalian target of rapamycin; **NRF2**: nuclear factor erythroid 2-related factor 2; **PI**: propidium iodide; **XRE**: xenobiotic response element.

***Corresponding author:** Janina M. Tomm, Department of Proteomics, Helmholtz-Centre for Environmental Research - UFZ, Permoser Str. 15, 04318 Leipzig, Germany. Phone number: +49-0341-2351819; Fax number: +49-0341-2351786; E-mail address: janina.tomm@ufz.de

1. Introduction

T cell development, subset lineage specification, survival and death are dependent on the initial step of T cell receptor activation [1]. Many major milestones in understanding this process originate from experiments with transformed T cell lines, such as Jurkat T cells [2]. Only very few proteomic studies focus on the activation of Jurkat cells. Those experiments either established new proteomic methods [3], or focused on detecting the protein composition of lipid rafts [4] and on elucidating general signaling pathways [5]. Thus the consequences of the different signaling patterns on the proteome are not well characterized yet. Furthermore, metabolomic processes are known to play an important role in T cell activation and differentiation [6].

The specific outcome of T cell stimulation is based on the integration of complex signals from the cellular microenvironment, which can be affected by environmental pollutants, such as B[*a*]P. Earlier findings showed that B[*a*]P and its metabolites influence cell mediated as well as humoral immunity [7] at rather low concentrations, but the mechanisms remain largely unknown. The chemical and biological inert B[*a*]P can be metabolically activated in the cell by three different pathways - the diol epoxide, the *o*-quinone and the radical cation pathway [8]. The cytochromes P4501A1/1B1, which are involved in the diol epoxide and *o*-quinone pathway, can be induced via AhR signaling [9]. Although it is known that some T lymphocytes, such as Th17 cells, express AhR at high levels, most of the other T helper cell subpopulations are reported to lack AhR [10, 11]. This led to the hypothesis of AhR-independent pathways causing the observed effects. One possible pathway is the activation of the transcription factor NRF2. Electrophilic compounds, such as those generated in the course of B[*a*]P transformation, directly or indirectly cause oxidative stress. This stress leads to the oxidation of the Kelch-like ECH-associated protein 1 (KEAP1), which then loses its ability to sequester NRF2 in the cytosol. After dissociation from KEAP1, NRF2 translocates into the nucleus and binds to ARE-elements. This binding activates the transcription of phase II detoxifying enzymes [12] and other proteins [13] that are partly redundant and partly complementary to the effects of the AhR signaling pathway.

In our previous experiments [14] and other studies about the effects of B[*a*]P on the proteome [15] mostly gel-based methods were applied. As the number of regulated proteins identified and quantified with this method is quite limited, we chose a GeLC-MS/MS setup this time. We were able to increase the number of identified and quantified proteins up to 2624 in total in comparison to 608 quantified and 112 identified protein spots in the previous study. Furthermore, our recent work showed strong evidence for alterations in metabolic pathways caused by B[*a*]P exposure in activated Jurkat T cells, especially in the glutamine metabolism [14]. Hence, we intensively examined the metabolomic changes with the help of FIA-MS/MS and IC-MS/MS in addition to proteomic alterations. We were able to analyze 183 metabolites in contrast to only 2 metabolites in the earlier study. Moreover, we investigated the effect of activation itself and the influence of B[*a*]P to gain deeper insights into the activation process and the toxicological effects of B[*a*]P on it. The proteome data were used to identify the involved cellular and metabolic pathways, which were verified and complemented by Western blotting and metabolomic analysis. Additionally, we analyzed the biotransformation of B[*a*]P in this cell line.

2. Material and Methods

2.1. *Activation and B[a]P exposure*

Jurkat T cells (clone E6-1, TIB-152, LGC Promochem, Wesel, Germany) were maintained as described earlier [16]. Four different treatments were performed: incubation with DMSO (control); exposure to B[*a*]P (B[*a*]P); activation and incubation with DMSO (activated); activation and exposure to B[*a*]P (activated + B[*a*]P). At first the cells were activated with 750 ng/ml ionomycin (IO) and 10 ng/ml phorbol-12-myristat-13-acetate (PMA) for 4 h or left untreated for the non-activated samples. Afterwards the cells were collected and resuspended in fresh medium supplemented with 50 nM B[*a*]P (all Sigma-Aldrich, Steinheim, Germany) dissolved in dimethylsulfoxide (DMSO; Applichem, Darmstadt, Germany) or fresh medium supplemented only with DMSO (for samples without B[*a*]P exposure). After B[*a*]P exposure for 24 h, all cells and supernatants were collected for all further analysis (except B[*a*]P metabolite analysis). All experiments were carried out in triplicates.

2.2. *Determination of cell viability and activation status*

After 4 h of activation and the following 24 h B[*a*]P exposure the viability and the activation status of the cells was analyzed by flow cytometry. 1 µl propidium iodide (Miltenyi Biotech, Bergisch Gladbach, Germany) or 1 µl annexin V-FITC (Abcam plc, Cambridge, UK) were used to stain $1x10^5$ cells for 5 min at room temperature to verify the viability of the cells. In order to determine the cell activation, $1x10^5$ cells were stained with 1 µl anti-CD25-PE (Miltenyi Biotech, Bergisch Gladbach, Germany) or 1 µl anti-CD69-PE (Immunotech, Marseille, France) at 4°C. The samples were measured on a FACSCalibur (Becton-Dickinson, Erembodegem, Belgium). The cell viability was assessed for all cells, whereas the activation markers were evaluated only for viable cells (based on cell size).

2.3. *Cell fractionation, 1D-SDS-PAGE and Western blotting*

For analysis with GeLC-MS/MS the cells were fractionated with the Qproteome Cell Compartment Kit (Qiagen, Hilden, Germany) as described previously [16].

A salt fractionation with increasing KCl concentrations (10, 200 and 400 mM) and different centrifugation steps with increasing velocity was performed to verify the expression of

NF-κB1 and phospho-eIF2α in different cellular compartments. All KCl buffers contained 10 mM HEPES, pH 7.4; 1.5 mM $MgCl_2$; 339 mM sucrose; 10% glycerol; 1x protease inhibitor (Roche, Mannheim, Germany) and the additions stated in brackets. After activation and B[*a*]P exposure the cells were washed two times with cold 1x PBS (5 min; 300 x g; 4°C). The volume of the packed cells was determined and the triple of that volume was used for all following buffers. The pellet was resuspended in 10 mM KCl buffer (0.1% Triton X-100; 10 mM KCl) and incubated on ice for 5 min. After centrifugation at 1,300 x g and 4°C for 5 min the supernatant was saved as 10 mM fraction (cytoplasm) and the pellet was solved in 200 mM KCl buffer (200 mM KCl) and incubated at 4°C for 60 min shaking at 850 rpm. The suspension was centrifuged at 15,000 x g and 4°C for 15 min and the supernatant was saved as 200 mM fraction. The pellet was dissolved in 400 mM KCl buffer (400 mM KCl) and again incubated at 4°C for 60 min shaking at 850 rpm. After a last centrifugation step at 15,000 x g and 4°C for 15 min the supernatant contained the 400 mM fraction. The pellet was resuspended in Benzonase buffer (50 mM Tris-HCl; 1 mM $MgCl_2$; 1x protease inhibitor) and 1 µl Benzonase (Novagen) was added. This mixture was incubated at 37°C for about 1.5 h with shaking (400 rpm) until the big clump of DNA and proteins was homogenized and saved as pellet fraction (nucleus). The protein content of all fractions was determined using the Pierce 660 nm Protein Assay (Thermo Fisher Scientific, Bonn, Germany) according to the manufacturer's instruction, but with 5 µl of all samples and standards. 30 µg of the indicated fractions from the salt fractionation were analyzed with immunoblots as described elsewhere [17]. Anti-NF-κB1 (1:200, #3035), anti-H2A (1:1000, #2578), anti-phospho-eIF2α (1:200, #3398, all Cell Signaling Technology) and anti-PSMA4 (1:100, H-128, Santa Cruz Biotechnology) were used as primary antibodies. Chemiluminescence signal was measured using Pierce ECL Western Blotting Substrate (Thermo Fisher Scientific, Bonn, Germany) on a FluorChem 8900 (Alpha Innotech). Immunoblot signals were quantified with ImageJ software (http://rsbweb.nih.gov/ij/). The content of cytoplasmic and nuclear proteins was normalized using the signals of the two 'housekeeping' proteins PSMA4 or H2A, respectively.

2.4. *Sample preparation, LC-MS/MS analysis and data processing*

The proteins were digested and analyzed with GeLC-MS/MS as described elsewhere [16]. The MS/MS data were evaluated with MaxQuant (version 1.2.2.5) using the human Uniprot database (version 11/16/2011). Carbamidomethylation of cysteine was specified as a fixed modification, whereas oxidation of methionine and acetylation of the protein N-terminus were specified as variable modifications. Peptide and protein FDR were set to 1%. A minimum of two peptides with at least one unique peptide was used for protein identification. Proteins were quantified by label-free quantification with a minimum ratio count of 1 and a match between runs time window of 4 min. The overall label-free quantification intensity of each sample was normalized to the average overall label-free quantification intensity of all samples from one fraction. Only proteins found in at least two of three replicates in all four different treatments were further analyzed. Fold changes were calculated between the label-free quantification intensities from the different treatments and a Student's t-test was conducted on the log2 label-free quantification intensities for each comparison. Proteins with a p-value less than 0.05 and an average linear fold change higher than 1.5 were considered as significantly regulated.

2.5. *Extraction and measurement of cellular metabolites*

Concentrations of 163 metabolites from cell lysates were determined using a targeted metabolic approach with the AbsoluteIDQ p150 kit (BIOCRATES Life Sciences AG, Innsbruck, Austria) as described earlier [18]. Briefly, extraction of cell pellets was carried out using 300 µl methanol/water (1/1 v/v) and ultrasonic homogenization for 2 min on ice. Samples were centrifuged and 30 µl of supernatants were prepared according to the manufacturer's protocol [19]. FIA-MS/MS analyses were carried out on an Agilent 1100 series binary HPLC system (Agilent Technologies, Waldbronn, Germany) coupled to an 4000 QTrap mass spectrometer (AB Sciex, Concord, Canada) equipped with a TurboIon spray source. Quantification was achieved by positive and negative multiple reaction monitoring (MRM) detection in combination with the use of stable isotope-labeled and other internal standards. Data evaluation for quantification of metabolite concentrations was performed with the MetIQ™ software package.

For IC-MS/MS analysis, extracts were diluted ten-fold in Milli-Q water and measured on an ICS-5000 (Thermo Fisher Scientific, Dreieich, Germany) coupled to an API 5500 QTrap (AB Sciex). Separation was achieved on an IonPac AS11-HC column (2 x 250mm, Thermo Fisher Scientific) with an increasing potassium hydroxide gradient. MS analysis was performed in MRM mode using negative electrospray ionization and included organic acids, carbohydrates and nucleotides involved in central metabolite pathways.

2.6. *Measurement of B[a]P and B[a]P metabolites*

Cell pellets from Jurkat T cells exposed to 50 nM, 5 µM, 10 µM and 50 µM B[*a*]P for 4 h and 24 h, were dissolved in 1 ml ethylacetate, homogenized and internal standards were added and vortexed for 2 min. The ethylacetate phase was evaporated and the residue was re-suspended in 50 µl methanol:water (1/1 v/v). 10 µl were injected into a Shimadzu LC-20 HPLC system (Shimadzu, Duisburg, Germany) coupled to an API 4000 QTrap mass spectrometer (AB Sciex). Chromatography was performed on an Envirosep PP column (125 mm × 2 mm, 5 µm particle size, Phenomenex, Aschaffenburg, Germany) at 20°C with a flow rate of 0.2 ml/

min using 5 mM ammonium acetate in methanol:water (1/1 v/v) and 5 mM ammonium acetate in methanol for gradient elution within 25 min. Analysis was conducted in the APCI mode (source temperature: 350°C) under MRM mode for quantification.

2.7. *Pathway analysis*

Proteins quantified in at least two out of the three replicates in all four treatments were analyzed further using IPA Ingenuity build 131235, version 11904312 (Ingenuity Systems, Inc., Redwood City, CA, USA). The analysis was performed using the preset parameters (see supplement) and excluding pathways related to cardiovascular signaling as well as neurotransmitter and other nervous system signaling.

2.8. *Metabolic network construction*

In order to integrate the content of the KEGG, EHMN and BiGG databases, identical compounds were merged based on common identifiers like KEGG IDs. Thereby, additional information on enzymes catalyzing identical biochemical reactions from the individual databases was preserved. Database-specific compounds that could not be mapped were built into the integrated metabolic network according to the reactions they participate in. The largest connected component of the integrated network was used for further analysis. It consisted of 3657 metabolite nodes and 5389 reaction nodes, and 45696 edges between the two node partitions.

2.9. *Subgraph extraction by k-walks algorithm*

In order to infer the relationships between the differentially regulated entities and to identify the metabolic pathways that are most relevant for the experimental condition, we mapped the lists of significantly regulated proteins from all three fractions as well as metabolites onto the integrated network. Given these significantly regulated species as seed nodes, the k-walks algorithm and a minimal threshold as described in [20] were applied to extract meaningful subgraphs from the metabolic network.

3. Results and discussion

3.1. *Influence of B[a]P exposure on the cell viability and activation status*

The cell viability and activation status of the Jurkat T cells was assessed after activation and B[*a*]P exposure by FACS measurement (Figure 1). In control cells and B[*a*]P treated cells, between 7 and 8% were annexin V or PI positive. Activated cells showed a fraction of 28% PI positive and 34% annexin V positive cells. In both, activated and non-activated cells, there was no difference in viability due to B[*a*]P exposure, indicating that a concentration of 50 nM B[*a*]P is not cytotoxic for Jurkat T cells within the time of exposure (24 h). The higher amount of apoptotic cells in the activated samples can be attributed to the known phenomenon of activation-induced cell death, a specific form of apoptosis initiated in previously activated T cells following restimulation via the T cell receptor complex [20]. A comparable number of around 30% apoptotic cells was measured by Chwae et al. in Jurkat T cells after stimulation with 100 ng/ml PMA and 1 g/ml ionomycin for 24 h [21].

Nearly all activated cells (with or without B[*a*]P exposure) were positive for the early activation marker CD69. In contrast, around 37% and 34% of the cells were CD25 positive in the activated and activated plus B[*a*]P exposed cells, respectively. For both activation markers, the amount of positive cells in non-activated and activated cells was slightly lower with B[*a*]P exposure, but the difference was not statistically significant. Our results are in line with experiments with lymphocytes isolated from blood, which showed about 30% CD25 and 80% CD69 positive cells after stimulation with PMA and IO [22].

3.2. *Biotransformation of B[a]P*

In addition to B[*a*]P itself, trans-B[*a*]P-7,8-dihydrodiol, trans-B[*a*]P-9,10-dihydrodiol, B[*a*]P-tetrahydrotetrol, B[*a*]P-1,6-dione as well as 3-OH-B[*a*]P, 7-OH-B[*a*]P, 8-OH-B[*a*]P were measured to investigate the corresponding degradation pathways in Jurkat T cells. Intracellular B[*a*]P was detected in all samples. However, the only metabolite found was B[*a*]P-

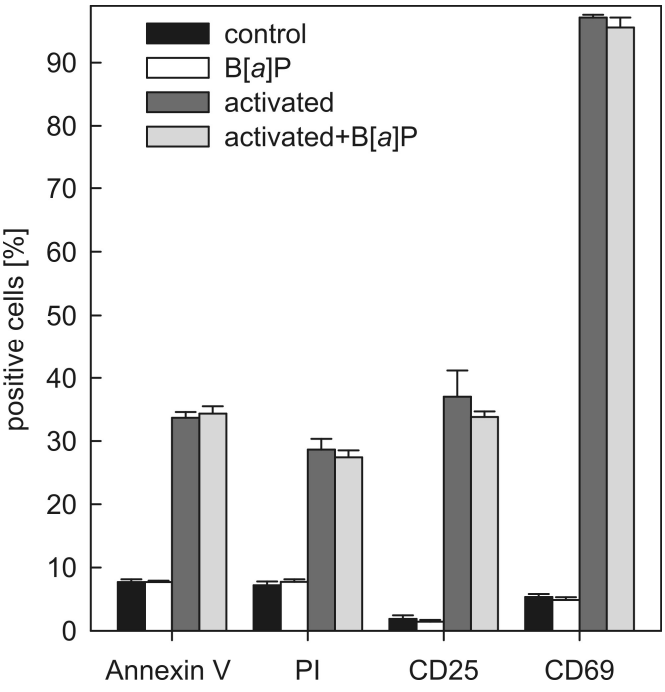

Figure 1. *Cell viability and activation status of Jurkat T cells after different treatments.* The viability and the activation status of the Jurkat T cells was analyzed by measurement of PI and annexin V staining as well as anti-CD25 or anti-CD69 staining via flow cytometry. Shown is the mean of three experiments ± SD.

1,6-dione (13.4 min). It was detected after exposure to 10 μM B[*a*]P for 4 h and 50 μM B[*a*]P for 4 h and 24 h (Figure S1) together with two other signals (13.7 min and 14.5 min) with the same MRM-transition (*m/z* 283->226). The data suggest that B[*a*]P is initially oxidized by P450 peroxidases or the monooxygenase catalytic cycle or by other peroxidases to form a B[*a*]P-cation. This reactive intermediate can either form DNA adducts or is metabolized further to B[*a*]P-1,6-dione.[8] The two unidentified peaks are likely to be other B[*a*]P-diones formed via the same metabolic pathway [23]. However, their further identification requires standard substances. For all other analyzed B[*a*]P-metabolites the concentrations were below the detection limit. Thus, it seems that in Jurkat cells B[*a*]P-dione formation via radical cation pathway is the main route of B[*a*]P-metabolism and –detoxification.

3.3. *Fractionation into different cellular compartments resulted in 2624 unambiguously identified proteins*

The proteome analysis yielded 2624 unambiguously identified proteins that were quantified by calculation of the peptide peak intensities (Table S1). With 1969 and 1842 hits, most of the proteins were found in the cytoplasm and membrane, respectively, whereas only 1506 proteins were identified in the nuclear fraction. In the cytoplasm and membrane fraction, similar numbers of proteins were quantified in all four different treatments, whereas in the nuclear fraction clearly more proteins (about 150 more) were quantified in the two activated samples. 1582 cytosolic, 970 nuclear and 1292 membrane proteins were used for enrichment and pathway analysis.

Based on the study of Beck *et al.* in 2011, which postulates a number of at least 10,000 proteins as typical for a human cell line [24], we achieved a reasonable coverage with a comparably simple fractionation method and only 108 LC-MS/MS runs. With the switch to a LC-MS/MS method we considerably improved the quantification rate compared to our previous B[*a*]P exposure experiments with Jurkat cells [14]. More precisely we identified and quantified in total 2624 proteins which is a 4-fold and 23-fold increase in comparison to the previously quantified and identified protein spots, respectively. The possibility of simultaneous identification and quantification of proteins by LC-MS is one of the clear advantages in comparison to gel-based approaches. Hence, the significance of subsequent pathway analysis is considerably improved.

In a global protein survey study on Jurkat T cells published in 2007, a total of 5381 proteins were identified with high confidence, but seven different cellular fractions, numerous replicates and about 16 times more LC-MS/MS runs than in our experiments had to be performed [25]. In respect to the nuclear fraction the number of 1506 detected proteins is higher than in another study that identified 872 proteins in the proteome of the T cell nucleolus [26]. De Wet *et al.* identified 1517 proteins in the T cell plasma membrane. In contrast, we were able to identify 325 additional proteins in the membrane fraction with more stringent identification criteria of at least two peptides and less LC-MS/MS runs as they cut every sample lane in ten pieces [27].

3.4. *Effects of activation and B[a]P on the proteome*

In order to understand the effect of activation on Jurkat T cells as well as the influence of B[*a*]P on this process, fold changes of the proteins as well as p-values were compared between the different treatments (Table S2). The significantly regulated proteins are visualized by plotting the log2 of the fold changes against the -log10 of the p-values (Figure 2A-D). B[*a*]P changes the expression of about 4% of the quantified proteins in the cytoplasm and membrane fraction (Figure 2E), whereas nearly no changes were detectable in the nuclear fraction (0.8%). Activation led to apparent changes of the protein abundance ranging from 5.3% to 16% in the three different cellular compartments in non-treated as well as in B[*a*]P exposed cells. Activation alone caused similar changes in the cytoplasm and nuclei fraction of about 12%, whereas activation in the presence of B[*a*]P modified the expression of nuclear proteins (16%) stronger than the expression of cytoplasmic proteins (9.2%). In addition, B[*a*]P exposure of activated cells caused only few significant changes in the proteome (0.9 - 1.4%) in all three fractions.

3.5. *Pathways influenced by activation and B[a]P exposure*

The abundance data from about 2500 proteins were analyzed using the Ingenuity Systems pathway program to unravel the affected cellular processes and pathways. The top ten regulated canonical pathways based on IPA p-values are summarized in Figure 3.

Effects of activation

Activation of Jurkat T cells affects the eIF2 pathway (Figure 3). Most of the quantified translation initiation factors and ribosomal proteins were down-regulated, and only very few were up-regulated. As the global regulation of translation mainly occurs by changes in the phosphorylation state of translation initiation factors [28], we analyzed the phosphorylation of eIF-2α (Figure 4A) and found that it was decreased in the activated cells. A reduced phosphorylation leads to an enhanced translation since the phosphorylation of eIF-2α inhibits the translation by blocking the GDP–GTP exchange on eIF2, which is required to reconstitute a functional complex for a new round of translation initiation [28]. This shows that changes in the protein abundance have to be carefully verified and that posttranslational modifications, especially phosphorylation, are very important for pathway regulation.

CD28 signaling in T helper cells is in the top ten of influenced pathways, which demonstrates on the proteomic level that the activation of the Jurkat cells was successful. Most of the proteins were found to be highly up-regulated, sometimes in several cellular fractions. NFKB1 and NFKB2 are induced by the CD28 co-stimulation pathway and play an important

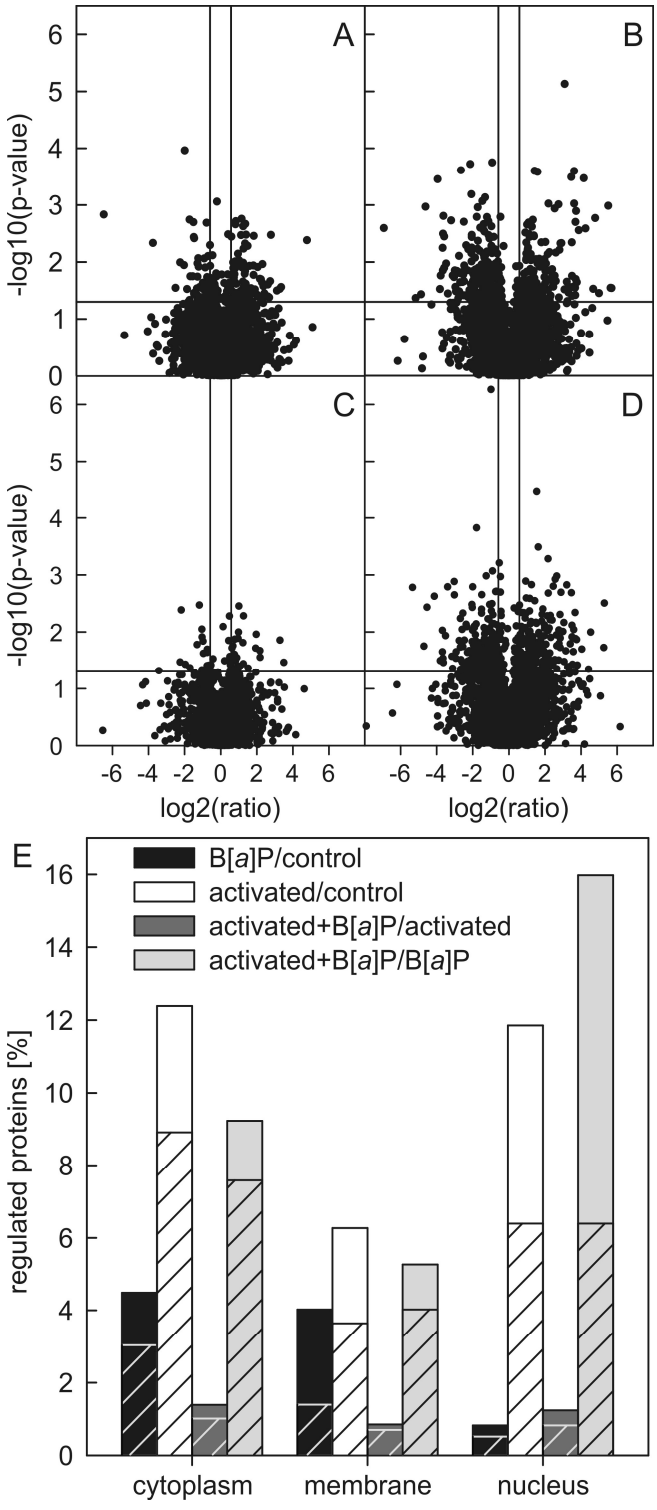

Figure 2. *Comparison of protein abundances between different treatments.* A-D: The log2 expression ratios are plotted against the -log10 of the p-values. The cutoffs for significantly changed proteins are indicated by solid lines (A - B[*a*]P/control; B - activated/control; C - activated+B[*a*]P/activated; D - activated+B[*a*]P/B[*a*]P); E: Shown is the distribution of differentially abundant proteins among the different compartments. Reduced protein abundance is illustrated by a fasciated pattern, increased protein abundance by no pattern.

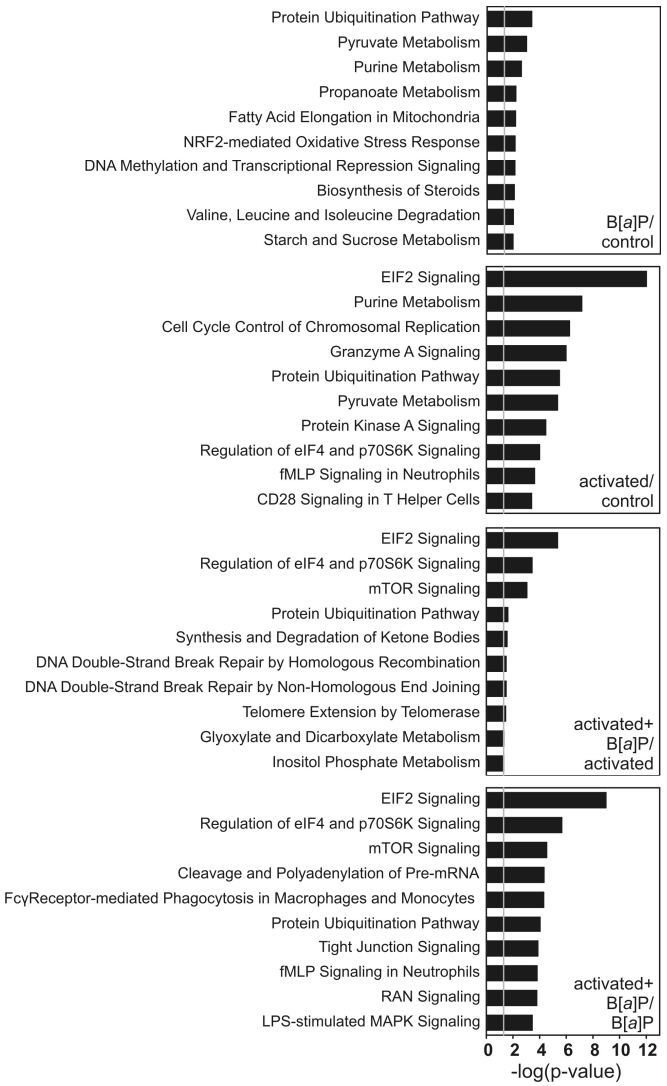

Figure 3. *Pathway analysis of proteins with Ingenuity IPA.* The bar chart displays the identified canonical pathways along with their significance (calculated by Ingenuity IPA). The top ten pathways are listed from most significant to least significant.

role in the regulation of the immune response, particularly for the transcription of cytokines such as IL-2 [29]. We verified the induced expression of NFKB1 by detecting its 120 kDa precursor as well as a substantial increase of the processed 50 kDa protein in the nucleus (Figure 4A). Furthermore, several actin-related proteins, α-actinin-1, vimentin and other proteins involved in reorganization of the cytoskeleton, were found to be significantly regulated. They are also important in T cell activation, especially in the formation of the immunological synapse [30].

Two metabolic pathways (purine and pyruvate metabolism) were identified and ranked within the top ten pathways by IPA. In order to confirm the results from pathway analysis we determined the concentrations of involved metabolites (Table S3). A significant down-regulation of AMP, ADP, ATP, UDP and UTP was observed and underlines the proteomic findings regarding nucleotide metabolism. In accordance

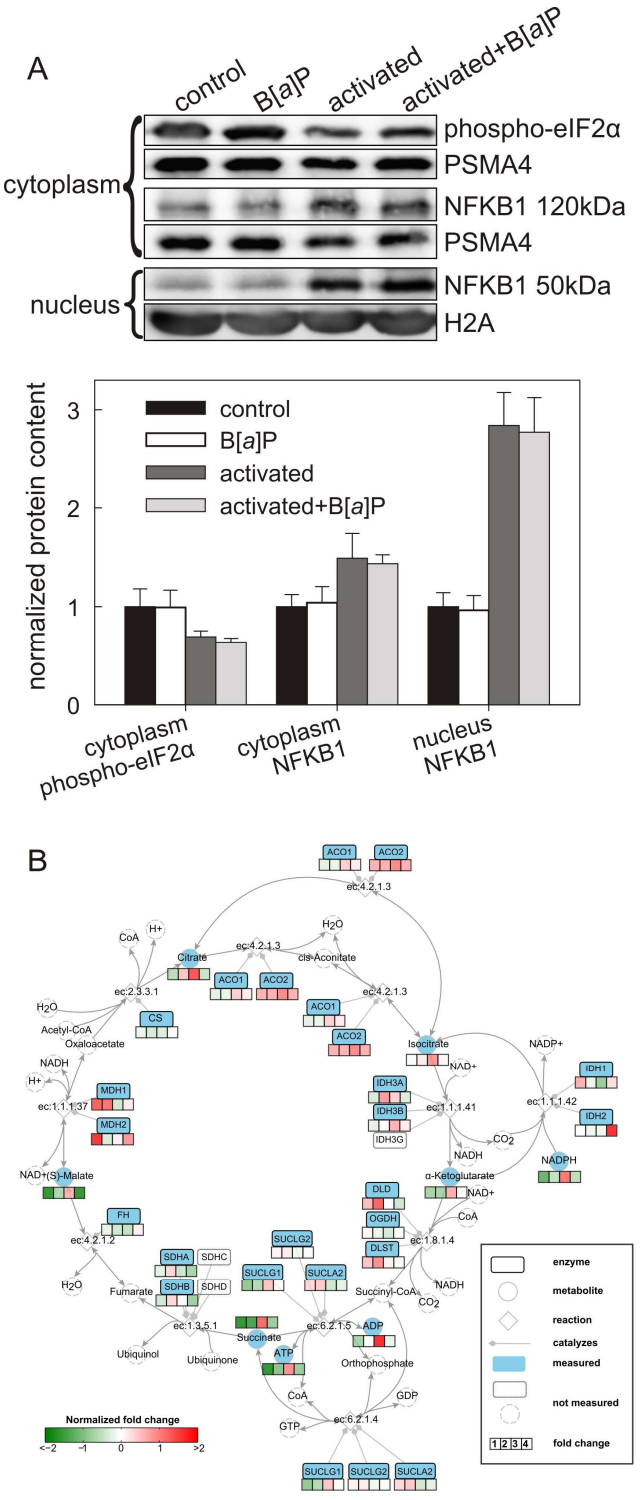

Figure 4. *Verification of proteomic results from LC-MS/M.* A: Shown are representative Western blots and the mean expression levels ± SD of NFKB1 and phospho-eIF2α from three replicates normalized to the indicated proteins used as input controls. B: Shown are the genes, metabolites and reactions involved in the citrate cycle. The normalized fold changes of the treatments are color -coded, which allows a comprehensible visualization of the integrated protein and metabolite data (1 - B[*a*]P/control; 2 - activated/control; 3 - activated+B[*a*]P/activated; 4 - activated+B[*a*]P/B[*a*]P).

to the influence of activation on the pyruvate metabolism, several enzymes and intermediates of the glycolysis such as hexokinase-1, phosphoenolpyruvate, glucose- and fructose 6-phosphate were up-regulated, although only pyruvate kinase isozymes M1/M2 and a subunit of the pyruvate dehydrogenase had a significantly increased expression. It is known that T cell stimulation leads to activation of the serine-threonine kinase AKT, which in turn promotes the localization of the glucose transporter GLUT1 to the membrane. This facilitates an increased glucose uptake, which was detected by a significant up-regulation of hexose concentration after activation [31]. Lactate and L-lactate dehydrogenase B chain were both significantly down-regulated, indicating that pyruvate may be metabolized in the citrate cycle rather than being dehydrogenated to lactate. Moreover, three intermediates of the citrate cycle, malate, succinate and α-ketoglutarate, were found to be down-regulated. Conversely, several citrate cycle enzymes were found to be induced, including the mitochondrial malate dehydrogenase. The opposite trends in regulation of enzymes and metabolites may be caused by the fact that the up-regulated enzymes efficiently metabolize their substrates and therefore their substrates are present in lower concentration, which is the case for malate and malate dehydrogenase. Glutamine, which was observed to be significantly up-regulated after T cell activation, can be deaminated in the mitochondria to generate α-ketoglutarate. This can be metabolized by the citrate cycle, regenerating the oxaloacetate required for continued biosynthesis. Even though glycolysis is regarded as the primary source of ATP generation in activated T cells, oxidative phosphorylation might represent an additional process for energy generation [32].

Effects of activation in the presence of B[a]P

According to IPA, the most striking effects of B[*a*]P on the activation process are changes in the pathway of cleavage and polyadenylation of pre-mRNA as well as in the mTOR and in the eIF4 and p70S6K signaling (Figure 3). The protein kinase mTOR acts as a central sensor and integrator of diverse environmental and metabolic influences. The best characterized downstream effectors of the mTOR signaling are the ribosomal protein p70S6K and eIF4EBP1. Both are phosphorylated in the activated mTOR pathway and promote translation initiation and therefore protein synthesis [33]. Furthermore, it is known that the mTOR signaling intersects with T cell metabolism and is involved in T cell fate decision and differentiation [6]. A disturbance in the mTOR pathway provoked by an environmental pollutant, such as B[*a*]P, could lead to an attenuation of the mTOR activity contributing to the down-regulation of T cell activity and even the induction of T cell anergy.

On the metabolic side we detected an increase of lysophosphatidylcholine concentrations after activation in the presence of B[*a*]P. Lysophosphatidylcholines play an important role in cell signaling via specific G-protein coupled receptors. It was shown that lysophosphatidylcholines activate the phos-

pholipase C, which releases diacylglycerols and IP_3, causing an increase in the intracellular Ca^{2+} concentration and the activation of the protein kinase C [34]. In addition, Okajima *et al.* demonstrated that the ability of IP_3 production in HL-60 leukemia cells depends on the fatty acid moieties of the phosphatidylcholines [35]. We detected significantly increased concentrations of 1-stearoyl lysophosphatidylcholine (lyso PC a C18:0) and additionally elevated levels of 1- lyso PC a C6:0, lyso PC a C14:0 and other lysophosphatidylcholines (fold changes 1.20 – 1.49).

In comparison to these results, the gel-based approach resulted in a more prominent identification of toxicological pathways such as AhR and NRF2 [14]. This is probably caused by the high abundance of proteins from these pathways (e.g. PRDX1, ACTB), which elevates the likeliness to detect them as affected proteins in gel-based approaches [36]. In contrast the effects on the mTor signaling and pre-mRNA processing found in this experiment depend as well on the quantification of less abundant proteins, again illustrating the value of LC-MS based approaches.

Effects of B[a]P exposure on non-activated cells

The B[*a*]P exposure of non-activated cells led to major changes in the cell metabolism as seven of the top ten pathways identified by Ingenuity are metabolic pathways (Figure 3). Several enzymes of the pyruvate, propanoate and fatty acid metabolism are up-regulated indicating a higher need for energy producing processes. Hexokinase-1, one of the key enzymes of glycolysis, which leads to pyruvate production, shows a 2.5-fold increased expression after B[*a*]P exposure. Hexokinases catalyze the ATP-dependent phosphorylation of glucose to yield glucose-6-phosphate and thereby control the first step of the glucose metabolism. Thus, they sustain the concentration gradient that permits facilitated glucose entry into cells and initiate all major pathways of glucose utilization [37]. In our previous work from Murugaiyan *et al.* we only identified the glutamine and pyrimidine metabolism as pathways affected by 50 nM B[*a*]P exposure in non-activated cells [14]. Hence, we obtained more detailed information about affected metabolic pathways in this new study.

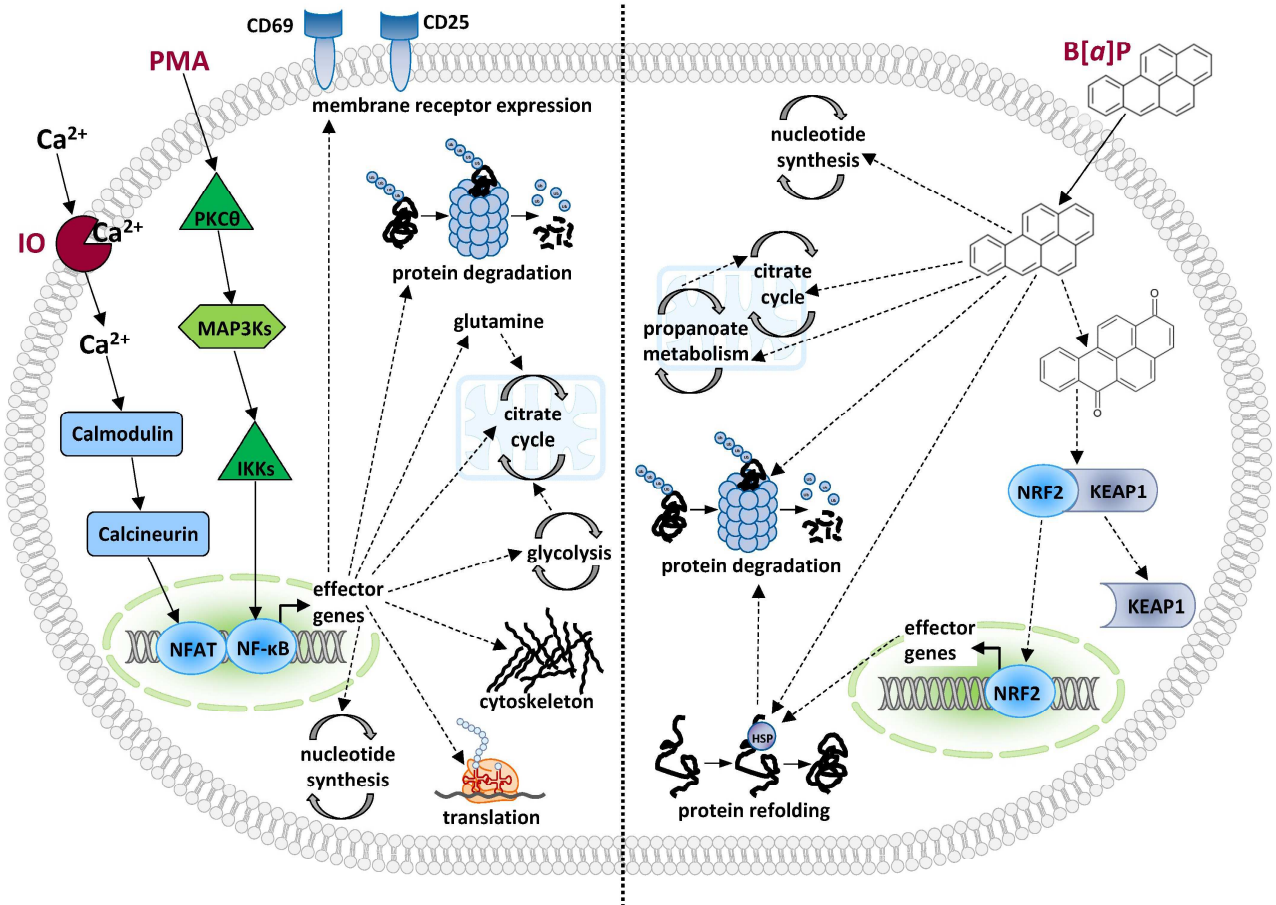

Figure 5. *Summary of signaling and metabolic pathways affected by activation and B[a]P exposure.* Shown is a summary of substances and intracellular pathways, which are affected by activation with PMA and IO (left side) or 50 nM B[*a*]P exposure (right side).

In order to further narrow down specifically affected areas in the metabolism, the integration of proteome and metabolome data was additionally performed by a random walks based approach. The enriched pathways and the corresponding biochemical connectivities between proteins and metabolites are shown in supplemental figure S2A-D. Since the citrate cycle was found to be affected under all examined treatments, it was chosen to illustrate the potential of integrated pathway analysis (Figure 4B). 22 different proteins covering nearly all reaction steps and the metabolites isocitrate, α-ketoglutarate, NADPH, ADP, ATP, succinate, malate and citrate as key molecules were detected. Three intermediates of the citrate cycle, malate, succinate and α-ketoglutarate, were found to be down-regulated. Conversely, several citrate cycle enzymes were found to be induced, including the mitochondrial malate dehydrogenase, indicating variations of enzyme activities rather than a simple abundance dependent correlation.

Our previous results indicated that B[*a*]P affects the IL-2 secretion as well as the glutamine and glutamate metabolism via the NRF2 pathway in Jurkat T cells [14]. Consistently, the NRF2 pathway is ranked on place six in this experiment, indicating a oxidative stress response after B[*a*]P exposure. Furthermore, we were able to show that B[*a*]P can be metabolized to B[*a*]P-quinones via the radical cation pathway. These quinones can undergo one-electron reduction by NAD(P)H-dependent reductases and form semiquinone anion radicals. The radicals redox-cycle back to diones in air and thereby generate ROS [9]. These reactive oxygen species can oxidize the disulfide bridges in KEAP1, which initiates the NRF2 pathway [38]. In addition to the transcriptional control of many phase I and phase II genes [12, 13] the NRF2 pathway can induce the expression of most proteasomal subunits [39] and heat shock proteins [40]. This connects it to the also identified ubiquitination pathway.

4. Concluding remarks

The effects of a subtoxic B[*a*]P concentration on activated and non-activated Jurkat T cells were revealed by proteomic and metabolomic profiling combined with pathway and network analysis. B[*a*]P is metabolized to B[*a*]P-1,6-dione and induces different metabolic pathways and the NRF2 pathway as a response to the electrophilic transformation products (Figure 5). Activation of Jurkat cells leads to pronounced changes, indicating strong adjustments in several metabolic pathways, protein and nucleotide synthesis (Figure 5). Although the effect of B[*a*]P is much stronger in non-activated cells, B[*a*]P seems to have an influence on the activation process suggesting an important role of the mTOR pathway in the cellular adaptation. The combined evaluation of proteome and metabolome data with an integrated, genome-scale metabolic model provided novel systems biological insights into the complex relation between metabolic and proteomic processes in Jurkat T cells during activation and subtoxic chemical exposure.

5. Supplementary material

Supplementary data and information is available at: http://www.jiomics.com/index.php/jio/rt/suppFiles/157/0

Supplemental Table 1 contains the protein identification and quantification data from MaxQuant.
Supplemental Table 2 shows the log-ratios and p-values of proteins for the four different comparisons. Only proteins identified in at least two of three replicates in all four treatments are listed.
Supplemental Table 3 shows the log-ratios and p-values of the quantified metabolites for the four different comparisons.
Supplemental Figure 1. MRM-chromatograms for the detection of B[*a*]P-1,6-dione using LCMS/MS.
Supplemental Figure 2. Metabolic subnetworks inferred from significantly changed proteins and metabolites by the kwalks approach.

Acknowledgments

This work was supported by the Helmholtz Impulse and Networking Fund through the Helmholtz Interdisciplinary Graduate School for Environmental Research (HIGRADE) and was funded in part by the European Research Council (starting grant 'LatentCauses'), by BMBF Grant no. 0315494A (project 'SysMBo') and by the DFG (SPP 'InKomBio'). The authors thank Silke Richter and Oliver Gericke for cooperation and technical assistance.

References

[1] D.D. Billadeau, J.C. Nolz, T.S. Gomez, Nat Rev Immunol, 7 (2007) 131-143. doi: 10.1038/nri2021

[2] R.T. Abraham, A. Weiss, Nat Rev Immunol, 4 (2004) 301-308. doi: 10.1038/nri1330

[3] E. Traxler, E. Bayer, J. Stockl, T. Mohr, C. Lenz, C. Gerner, Proteomics, 4 (2004) 1314-1323. doi: 10.1002/pmic.200300774

[4] M. Kobayashi, T. Katagiri, H. Kosako, N. Iida, S. Hattori, Electrophoresis, 28 (2007) 2035-2043. doi: 10.1002/elps.200600675

[5] V. Mayya, D.H. Lundgren, S.I. Hwang, K. Rezaul, L. Wu, J.K. Eng, V. Rodionov, D.K. Han, Sci Signal, 2 (2009) ra46. doi: 10.1126/scisignal.2000007

[6] K. Yang, H. Chi, Semin Immunol, 24 (2012) 421-428. doi: 10.1016/j.smim.2012.12.004

[7] P. Urso, N. Gengozian, R.M. Rossi, R.A. Johnson, J Immunopharmacol, 8 (1986) 223-241.

[8] D. Lu, R.G. Harvey, I.A. Blair, T.M. Penning, Chem Res Toxicol, 24 (2011) 1905-1914. doi: 10.1021/tx2002614

[9] H. Jiang, S.L. Gelhaus, D. Mangal, R.G. Harvey, I.A. Blair, T.M. Penning, Chem Res Toxicol, 20 (2007) 1331-1341. doi: 10.1021/tx700107z

[10] C. Esser, A. Rannug, B. Stockinger, Trends Immunol, 30 (2009) 447-454. doi: 10.1016/j.it.2009.06.005

[11] M. Veldhoen, J.H. Duarte, Curr Opin Immunol, 22 (2010) 747-752. doi: 10.1016/j.coi.2010.09.001

[12] M.E. Burczynski, T.M. Penning, Cancer Res, 60 (2000) 908-915.

[13] V.O. Tkachev, E.B. Menshchikova, N.K. Zenkov, Biochemistry (Mosc), 76 (2011) 407-422.

[14] J. Murugaiyan, M. Rockstroh, J. Wagner, S. Baumann, K. Schorsch, S. Trump, I. Lehmann, M. Bergen, J.M. Tomm, Toxicol Appl Pharmacol, 269 (2013) 307-316. doi: 10.1016/j.taap.2013.03.032

[15] F. Dautel, S. Kalkhof, S. Trump, J. Michaelson, A. Beyer, I. Lehmann, M. von Bergen, J Proteome Res, 10 (2011) 379-393. doi: 10.1021/pr100723d

[16] M. Rockstroh, S.A. Müller, C. Jende, A. Kerzhner, M. von Bergen, J.M. Tomm, JIOMICS, 1 (2011) 135-143.

[17] N. Morbt, J. Tomm, R. Feltens, I. Mogel, S. Kalkhof, K. Murugesan, H. Wirth, C. Vogt, H. Binder, I. Lehmann, M. von Bergen, J Proteome Res, 10 (2011) 363-378. doi: 10.1021/pr1005718

[18] A. Oberbach, M. Bluher, H. Wirth, H. Till, P. Kovacs, Y. Kullnick, N. Schlichting, J.M. Tomm, U. Rolle-Kampczyk, J. Murugaiyan, H. Binder, A. Dietrich, M. von Bergen, J Proteome Res, 10 (2011) 4769-4788. doi: 10.1021/pr2005555

[19] W. Röhmisch-Margl, C. Prehn, R. Bogumil, C. Röhring, K. Suhre, J. Adamski, Metabolomics, 8 (2011) 133-142.

[20] D.R. Green, N. Droin, M. Pinkoski, Immunol Rev, 193 (2003) 70-81.

[21] Y.J. Chwae, M.J. Chang, S.M. Park, H. Yoon, H.J. Park, S.J. Kim, J. Kim, J Immunol, 169 (2002) 3726-3735.

[22] M. Reddy, E. Eirikis, C. Davis, H.M. Davis, U. Prabhakar, J Immunol Methods, 293 (2004) 127-142. doi: 10.1016/j.jim.2004.07.006

[23] M. Huang, I.A. Blair, T.M. Penning, Chem Res Toxicol, 26 (2013) 685-692. doi: 10.1021/tx300476m

[24] M. Beck, A. Schmidt, J. Malmstroem, M. Claassen, A. Ori, A. Szymborska, F. Herzog, O. Rinner, J. Ellenberg, R. Aebersold, Mol Syst Biol, 7 (2011) 549. doi: 10.1038/msb.2011.82

[25] L. Wu, S.I. Hwang, K. Rezaul, L.J. Lu, V. Mayya, M. Gerstein, J.K. Eng, D.H. Lundgren, D.K. Han, Mol Cell Proteomics, 6 (2007) 1343-1353. doi: 10.1074/mcp.M700017-MCP200

[26] M.A. Jarboui, K. Wynne, G. Elia, W.W. Hall, V.W. Gautier, Mol Immunol, 49 (2011) 441-452. doi: 10.1016/j.molimm.2011.09.005

[27] B. de Wet, T. Zech, M. Salek, O. Acuto, T. Harder, J Biol Chem, 286 (2011) 4072-4080. doi: 10.1074/jbc.M110.165415

[28] F. Gebauer, M.W. Hentze, Nat Rev Mol Cell Biol, 5 (2004) 827-835. doi: 10.1038/nrm1488

[29] L. Tuosto, Immunol Lett, 135 (2011) 1-9. doi: 10.1016/j.imlet.2010.09.005

[30] J.K. Burkhardt, E. Carrizosa, M.H. Shaffer, Annu Rev Immunol, 26 (2008) 233-259. doi: 10.1146/annurev.immunol.26.021607.090347

[31] C. Mauro, H. Fu, F.M. Marelli-Berg, Curr Opin Pharmacol, 12 (2012) 452-457. doi: 10.1016/j.coph.2012.02.018

[32] R.G. Jones, C.B. Thompson, Immunity, 27 (2007) 173-178. doi:10.1016/j.immuni.2007.07.008

[33] B. Magnuson, B. Ekim, D.C. Fingar, Biochem J, 441 (2012) 1-21. doi: 10.1042/BJ20110892

[34] Y. Xu, Biochim Biophys Acta, 1582 (2002) 81-88.

[35] F. Okajima, K. Sato, H. Tomura, A. Kuwabara, H. Nochi, K. Tamoto, Y. Kondo, Y. Tokumitsu, M. Ui, Biochem J, 336 (Pt 2) (1998) 491-500.

[36] P. Wang, F.G. Bouwman, E.C. Mariman, Proteomics, 9 (2009) 2955-2966. doi: 10.1002/pmic.200800826

[37] R.B. Robey, N. Hay, Oncogene, 25 (2006) 4683-4696. doi: 10.1038/sj.onc.1209595

[38] P.M. Nguyen, M.S. Park, M. Chow, J.H. Chang, L. Wrischnik, W.K. Chan, Toxicol Sci, 116 (2010) 549-561. doi: 10.1093/toxsci/kfq150

[39] M.K. Kwak, N. Wakabayashi, J.L. Greenlaw, M. Yamamoto, T.W. Kensler, Mol Cell Biol, 23 (2003) 8786-8794.

[40] T. Rangasamy, C.Y. Cho, R.K. Thimmulappa, L. Zhen, S.S. Srisuma, T.W. Kensler, M. Yamamoto, I. Petrache, R.M. Tuder, S. Biswal, J Clin Invest, 114 (2004) 1248-1259. doi: 10.1172/JCI21146